THE JOURNAL OF PHYSICAL CHEMISTRY B

Article

pubs.acs.org/JPCB

Self-Assembly of Gemini Surfactants: A Computer Simulation Study

Jagannath Mondal, Mahesh Mahanthappa, and Arun Yethiraj*

Department of Chemistry, University of Wisconsin, Madison, Wisconsin 53706, United States

ABSTRACT: The self-assembly behavior of gemini (dimeric or twin-tail) dicarboxylate disodium surfactants is studied using molecular dynamics simulations. A united atom model is employed for the surfactants with fully atomistic counterions and water. This gemini architecture, in which two single tailed surfactants are joined through a flexible hydrophobic linker, has been shown to exhibit concentration-dependent aqueous self-assembly into lyotropic phases including hexagonal, gyroid, and lamellar morphologies. Our simulations reproduce the experimentally observed phases at similar amphiphile concentrations in water, including the unusual ability of these surfactants to form gyroid phases over unprecedentedly large amphiphile concentration windows. We demonstrate quantitative agreement between the predicted and experimentally observed domain spacings of these nanostructured materials. Through careful conformation analyses of the surfactant molecules, we show that the gyroid phase is electrostatically stabilized related to the lamellar phase. By starting with a lamellar phase, we show that use of a bulkier $N(CH_3)_4^+$ counterion in place of Na^+ drives the formation of a gyroid phase. Decreasing the charge on the surfactant headgroups by carboxylate protonation decreases the degree of order in the lamellar phase. Using our models, we show that the translational diffusion of water and the Na^+ counterions is decreased by several orders of magnitude over the studied concentration range, and we attribute these effects to strong correlations between the mobile species and the surfactant headgroups.

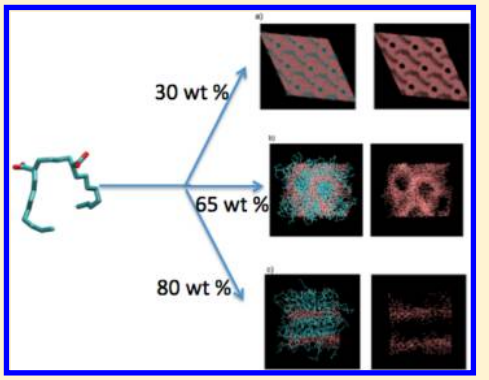

1. INTRODUCTION

A delicate balance of noncovalent interactions drives the assembly of hydrated small molecule amphiphiles into materials with periodic, long-range nanoscale order. Understanding the factors that govern amphiphile self-assembly is of fundamental importance, and the unique physical properties of these aqueous lyotropic liquid crystals (LLCs) is of practical importance.[1] These materials have attracted attention[2,3] as structure directing agents in a number of applications including the synthesis of mesoporous materials,[4,5] protein crystallization media,[6] and new membranes.[7,8] In this paper, we study the self-assembly of a class of amphiphilic molecules, called gemini surfactants,[9] using molecular dynamics simulations.

Lyotropic liquid crystal phases are interesting because of the variety of morphologies they exhibit and for the distinct nature of the domains in the phases.[1,10] LLC phases include lamellar (L_α), bicontinuous cubic (Q, e.g., double gyroid and double diamond), hexagonally packed cylinders (H), and discontinuous cubic (I, e.g., spherical micelles arranged on a body-centered cubic lattice) morphologies. These phases contain distinct nanoscale hydrophobic and hydrophilic domains, with periodic translational order, where the interfaces between the domains are decorated with the hydrophilic headgroup of the small molecule surfactant.

The structure of the hydrophobic portion of the amphiphile as well as the surfactant headgroup and counterion are known to dramatically influence the observed LLC morphology and consequent bulk properties, even within structurally similar small molecule amphiphiles.[11,12] LLC systems are therefore a useful platform for probing the fundamental nature of self-assembly. The spatial structure of the hydrophilic domains also makes this a good system to study the static and dynamic properties of nanoconfined water.[13]

The LLC phase behavior of gemini (or "twin-tail") surfactants has generated recent interest because of the unusually large range of concentrations for which they exhibit bicontinuous cubic morphologies.[11,12] Gemini surfactants are comprised of two single-tail surfactants dimerized through a flexible hydrophobic linker near the headgroups (see Figure 1).[9] In addition to the propensity to form network morphologies, the stability and ordered state symmetries of LLCs derived from gemini surfactants depend quite sensitively upon the counterion as well as the linker and alkyl tail lengths.

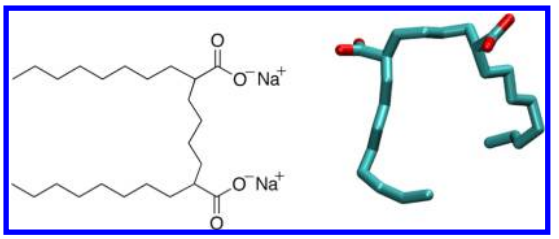

Figure 1. Chemical formula and united atom representation of the gemini surfactant Na-74.

Special Issue: Paul F. Barbara Memorial Issue

Received: May 21, 2012
Revised: August 30, 2012

   dx.doi.org/10.1021/jp304933k | J. Phys. Chem. B XXXX, XXX, XXX–XXX

A recent report by Sorenson et al. described the aqueous LLC phase behavior of gemini dicarboxylate surfactants, which readily form gyroid ($Ia\bar{3}d$ or space group #230 symmetry) and primitive ($Im\bar{3}m$ or space group #229 symmetry) network phases over unusually large amphiphile concentration windows (~10−20 wt % amphiphile wide) with unusually high thermal stabilities (up to 100 °C).[11] This finding is significant because Q-phases typically exist only in limited water concentration and temperature phase windows, due to the fact that their interfaces deviate substantially from a constant mean interfacial curvature.[14,15] While "critical packing parameter" models enable correlations of amphiphile structure with the formation of constant mean curvature L_α, H, and I phases, these models fail to provide reliable and general molecular design criteria for amphiphiles that form nonconstant mean curvature Q-phases.[16,17] Hence, no simple framework for understanding the aqueous LLC self-assembly characteristics of gemini surfactants exists.

Given the small domain sizes associated with lyotropic self-assembly of small molecule surfactants, computational studies of their self-assembly should be feasible. However, only a few simulations of gemini surfactants have been previously reported. To the best of our knowledge, no simulations with chemically realistic models have examined the formation of LLC phases. Karaborni et al.[18] performed simulations with a generic model and showed that these molecules do form lyotropic phases, in contrast to their single-tail analogues. Atomistic studies of gemini surfactants (using at most 20 molecules) have examined the behavior of gemini amphiphiles at interfaces,[19−21] their ability to form electrostatically bound complexes with charged polymers,[22] and their properties as single molecules in solution.[23] Shinoda et al.[24] performed simulations of a coarse-grained model of double-tailed ethylene glycol surfactants and reported micellar, hexagonal, and lamellar phases. In their model, three water molecules were represented by a single nonpolar Lennard-Jones site, and each site on the surfactant represented a group with either two or three heavy atoms.

In this work, we examine the LLC phase behavior of gemini surfactants using computational methods. We specifically focus on the aqueous LLC self-assembly of the gemini dicarboxylate surfactant docosane-9,14-dicarboxylate disodium salt (Na-74; Figure 1). As previously reported by Mahanthappa and co-workers,[11] this surfactant forms stable hexagonally packed cylinder morphologies between 30 and 50 wt % Na-74 in water, gyroid phases in the range 55−70 wt % Na-74, and lamellar phases between 75 and 90 wt % Na-74 in water.

By employing a combination of a united atom representation of the surfactants with atomistic sodium counterions and water, we show that existing force fields reproduce the experimentally observed phase behavior. These calculations predict the experimentally observed morphologies as a function of amphiphile concentration while also furnishing quantitatively accurate predictions of the characteristic domain spacings that have been experimentally determined using small-angle X-ray scattering. On the basis of these successes, we subsequently use our models to obtain more detailed insights into why these surfactants adopt these complex network morphologies with nonconstant mean curvature interfaces. Specifically, conformational analyses of the surfactant molecules demonstrate that gemini amphiphile self-assembly into gyroid phases is driven by electrostatic interactions between the tethered surfactant headgroups. Furthermore, our models enable predictions of the partial pair correlation functions, local environments near the surfactant headgroups, and the residence times of various species at the hydrophilic−hydrophobic domain interfaces.

The rest of this paper is organized as follows: the simulation model and methods are described in section II, results are presented in section III, and some conclusions are presented in section IV.

2. SIMULATION MODEL AND METHODS

We use the GROMOS96 united atom forcefield GROMOS45a3[25] for the gemini surfactant, where hydrogen atoms are not treated explicitly. The force field contains parameters for CH, CH_2, and CH_3 groups and the oxygen atoms. We use the SPC model for water[26] (which is compatible with GROMOS force field) and GROMOS compatible force field parameters for the counterions.[27] Molecular dynamics simulations are performed using the GROMACS-4.0.7 software package.[28] The SETTLE[29] algorithm is used to keep the water molecules rigid.

Simulations are performed for three concentrations, 30, 65, and 80% by weight of surfactants which correspond to 60, 13, and 6.2 water molecules per surfactant molecule, respectively. Initial configurations are generated taking into account the expected phase (which is known from experiment). For 30 and 80 wt %, we use 100 surfactant molecules, and for 65 wt %, we use 250 surfactant molecules to ensure correct box size. The size and shape of the simulation cell depend on the concentration. For 30 wt %, the cell is anistropic and has dimensions of 8.68 nm × 7.52 nm × 3.82 nm; for 65 and 80 wt %, the simulation cell is cubic with a linear dimension of 6.4 and 4.41 nm, respectively. The surfactant molecules are randomly inserted into the cubic simulation cell followed by the water molecules and the counterions.

The system is evolved using a leapfrog algorithm with a time step of 3 fs. Lennard-Jones (LJ) interactions are switched smoothly to zero at 1.0 nm, and the particle-mesh Ewald (PME) summation[30,31] is used for the long-range electrostatic interactions. The PME parameters are as follows: real space cutoff distance of 1.4 nm and interpolation order of 6, with a maximum fast Fourier transform grid spacing of 0.12 nm. Each of the initial configurations is subjected to energy-minimization using the steepest-descent technique followed by a short equilibration molecular dynamics (MD) simulation in the NPT ensemble at 300 K and 1 atmospheric pressure. A Berendsen thermostat[32] is used to keep the average temperature constant with the surfactants and water (along with counterions) coupled separately with the thermostat. Pressure is controlled with a Berendsen barostat.[32]

The simulation protocol is different for the three concentrations studied. An isotropic pressure coupling is used at the two higher concentrations, but an anisotropic pressure coupling is used for the lowest concentration, as recommended by Marrink et al.[33] This allows the simulation cell to change shape to accommodate the hexagonal phase. For the intermediate concentration (where a gyroid morphology is expected) after equilibration in the NPT ensemble, simulations are performed in the NVT ensemble.

In computer simulations, because of the finite size of the simulation cell, the shape of the cell and simulation protocols can restrict the morphologies that will be observed. For example, if an isotropic pressure coupling is used, the cubic phase is always observed instead of a hexagonal phase, but an anisotropic pressure coupling allows the formation of both phases.[33] The situation is tricky for bicontinuous phases where

dx.doi.org/10.1021/jp304933k | J. Phys. Chem. B XXXX, XXX, XXX−XXX

the periodicity of the phase has to be commensurate with the periodic boundary conditions. As has been pointed out by Escobedo and co-workers,[34] the simulation cell size has to be chosen carefully to avoid the formation of other metastable morphologies instead of the gyroid phase. In general, the periodic length of the simulation cell is chosen by trial and error to allow for the gyroid phase to develop. In this work, we estimate the "correct" box size, which turns out to be 6.4 nm at 65 wt % of surfactant, from the experimental scattering vector. The shape and size of the simulation cell is not an issue, however, for the stability of the lamellar phase. Given the sensitivity of the observed phases to the initial configuration and simulation protocol, we do not claim to discover new phases but rather merely reproduce phases that are observed in experiment.

The simulation duration is different depending on the concentration. For 30 wt %, a 200 ns simulation is sufficient, and for 65 and 80 wt %, simulations of 1000−1300 ns are necessary. In every case, four independent initial configurations are generated and four independent simulations are performed.

In order to compare the results with the case of infinitely dilute solution, a separate simulation is performed by solvating a single surfactant molecule with water molecules in a cubic box of linear dimension of 3.5 nm. Two counterions are added to maintain electroneutrality. The system is equilibrated for 10 ns, and ensemble averages are calculated over a 50 ns simulation.

The structure factor is calculated using the g_rdf utility in GROMACS. The primary simulation cell is replicated twice in each dimension, and the intensity is calculated from the structure factor using the Cromer−Mann formula.[35] In this procedure, the atomic scattering factor, f_k, of the kth atom is given by

$$f_k(q) = c + \sum_{k=1}^{4} a_k \exp\left(-b_k \sin^2 \frac{\theta}{\lambda}\right) \quad (1)$$

where $q = (4\pi/\lambda)\sin(\theta/2)$ is the magnitude of the momentum transfer variable, λ is the wavelength of incident radiation, θ is half the angle between incoming and scattered radiation, and a_k, b_k, and c are empirical fit parameters which are tabulated elsewhere.[35] The structure factor is given by

$$S(q) = \sum_k f_k(q) \exp(\imath \mathbf{q}\cdot\mathbf{r}) \quad (2)$$

where $\mathbf{q}$ and $\mathbf{r}$ are the momentum transfer variable and position in space, respectively, and the sum is over all atoms. The scattering intensity is given by

$$I(q) = |S(q)|^2 \quad (3)$$

3. RESULTS AND DISCUSSION

The simulations reproduce the experimentally observed phases at the concentrations studied; i.e., hexagonal, gyroid, and lamellar phases are observed at 30, 65, and 80 wt %, respectively. Figure 2 depicts snapshots from the simulations in the three cases in which the three morphologies are clearly seen. As the concentration of surfactant is increased, the morphology tends toward decreasing the curvature of the surfactant phase, consistent with experiment. At 65 wt %, the morphology is bicontinuous with percolating water regions. Note that these snapshots are all formed from self-assembly of a system with water and surfactant molecules inserted randomly into a box. We are aware of only one previous study (on lipid molecules)[36] where such spontaneous self-assembly into lyotropic phases was observed.

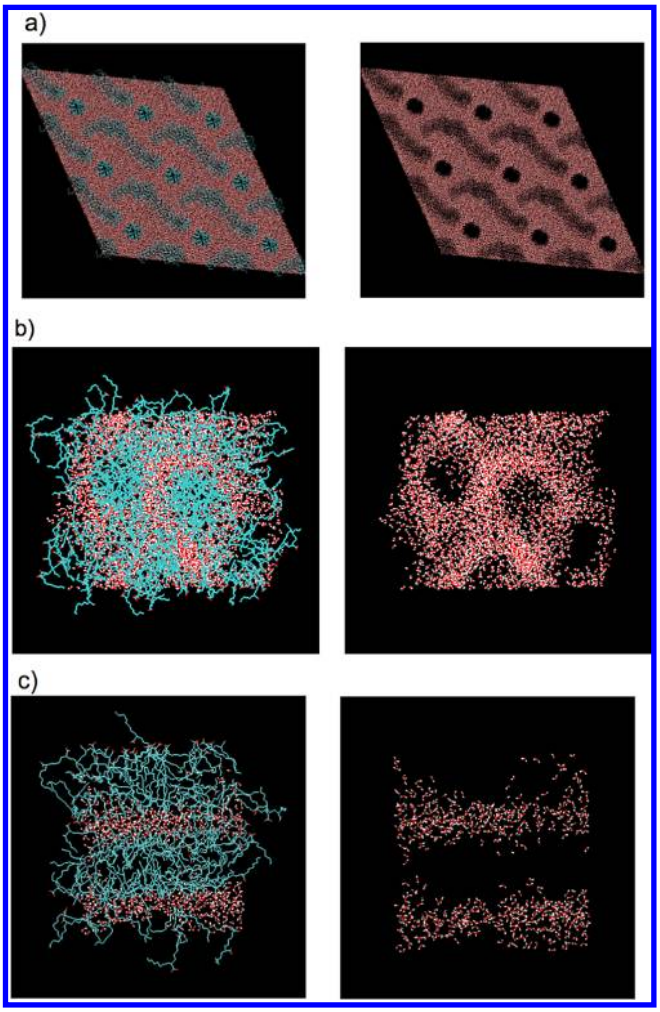

Figure 2. Representative snapshots of the simulation cell for (a) hexagonal phase at 30 wt %, (b) gyroid phase at 65 wt %, and (c) lamellar phase at 80 wt % of the surfactants. The left panel shows the system with surfactants (blue) and water (red), and the right panel shows only the water molecules. In parts b and c, only the primary simulation cell is depicted, but eight periodic images are included in part a.

The scattering intensity obtained from computer simulations is in reasonable agreement with small-angle X-ray scattering data. Figure 3 depicts the scattering intensity obtained from the simulations at the three concentrations; also shown are the experimental results. The small size of the simulation cell restricts the values of wavevectors accessible, and the peaks in the scattering intensity are not as sharp. For the hexagonal phase, the peak positions are 0.14 and 0.37 Å^{-1} in the simulations and 0.20 and 0.35 Å^{-1} in experiment. For the gyroid phase, the peak positions are 0.2 and 0.29 Å^{-1} in the simulations and 0.23 and 0.26 Å^{-1} in experiment. For the lamellar phase, the peak position is 0.28 Å^{-1} in simulations and 0.27 Å^{-1} in experiment. In all cases except for the lower angle peak for the hexagonal phase, the simulation results are in semiquantitative agreement with experiment. We attribute the disagreement at low wave vectors to the finite size of the simulation cell.

The conformations of the surfactants are markedly different in the lyotropic liquid crystalline phases when compared to the

dx.doi.org/10.1021/jp304933k | J. Phys. Chem. B XXXX, XXX, XXX−XXX

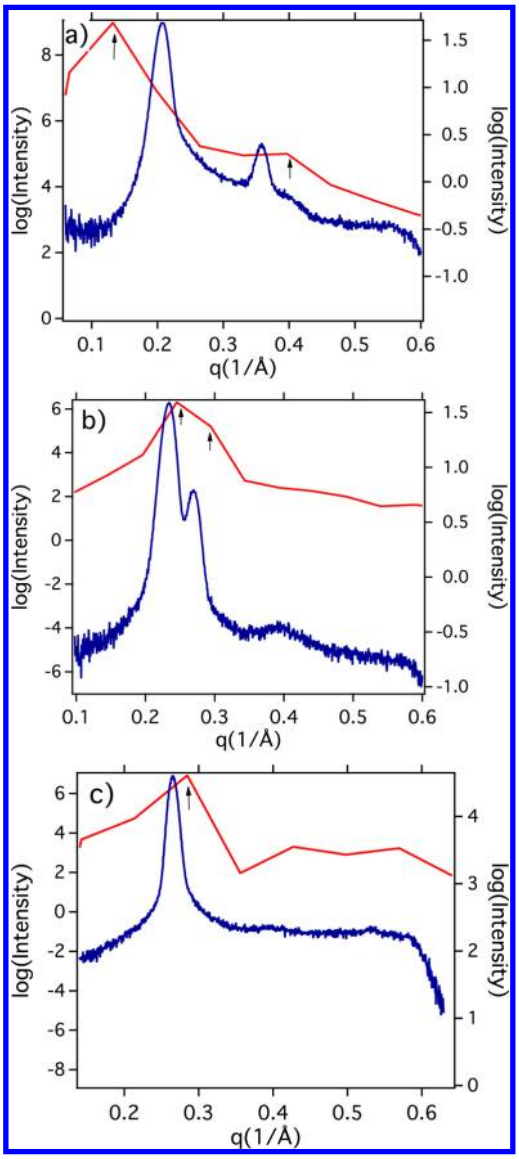

Figure 3. Simulation results (red curve, left scale) and corresponding experimental results (blue curve, right scale) for the scattering intensity for (a) 30 wt %, (b) 65 wt %, and (c) 80 wt %. The arrows point to the position of the peak in the simulation that we identify with the peak seen in experiment.

conformations at infinite dilution. Figure 4 compares the probability distribution functions for three characteristic distances: end-to-end distance of the tails (R_E) and bridge (R_B) and the distance (R_{EE}) between the end points of the two tails on the surfactant. At infinite dilution, all of these distributions are broad, showing that there is significant conformational freedom for the molecules. The distributions are much sharper in the lyotropic phases than at infinite dilution. There is little difference in the end-to-end distance distribution of the tails and the bridge (Figure 4a and b) in the different lyotropic phases: the distribution is sharply peaked at a distance of 0.88 and 0.37 nm, respectively. For fully stretched (all-trans) chains, the end-to-end distance for the tails (8 bonds) and bridge (5 bonds) is approximately 1 and 0.63 nm, respectively. The tails are therefore stretched out, but the bridge compacted to about 58% of its maximum length. The ends of the tails are closer to each other in the hexagonal phase than in the gyroid and lamellar phase. This is reasonable because the lower volume in the interior of the cylinder pushes the tails closer together than in the gyroid and lamellar phase. The peak in $P(R_{EE})$ occurs at distances much larger than that in $P(R_B)$ because the tails are stretched but are spread at different angles relative to the bridge. An examination of distribution of angles between the tails shows that, in all cases, the tails are on the same side of the bridge, which is expected because both the tails are in the hydrophobic domain and the headgroups are at the interface. The bond angle between the first bond of the tail and the bridge is close to the equilibrium value of 109° in all but the hexagonal phase where it is smaller. One can estimate the average angle between the tails (about the axis represented by the bridge) from the lengths of the tails and the distance R_{EE} between the ends of the tails. If we use the most probable value for R_E and R_{EE} (Figure 4), we estimate that the tails are spread at angles of roughly 45° from the normal (on either side of the bridge) in the hexagonal phase and 60° from the normal in the other two lyotropic phases.

Interestingly, the conformational properties of the surfactants are very similar in the lamellar and gyroid phases; the most probable values of R_E, R_B, and R_{EE} are almost identical. Note that $P(R_E)$, $P(R_B)$, and $P(R_{EE})$ are *more* sharply peaked in the gyroid (compared to the lamellar) phase. This is contrary to the notion that the gyroid phase is stable because these molecules can tolerate greater local curvature in the microphases, as previously suggested by Sorenson et al.[11] If the molecular conformations were adjusting to the local curvature, one would expect broader distributions in the gyroid phase, which is the opposite of what we observe.

For convenience in analyzing pair correlations, we group the atoms of the surfactant into two groups: Tail (T) refers to all sites on the tails of the surfactant, head (H) refers to oxygen atoms in the two carboxylate groups, oxygen water (OW) refers to the oxygen atom of a water molecule, and the atoms in the counterions (C) are grouped together.

The spatial correlation between different water molecules and between water molecules and counterions increases as the surfactant concentration is increased. Parts a and b of Figure 5 depict the radial distribution function between the oxygen atoms on different water molecules and between the water oxygen and counterions, respectively. As the concentration is increased, the first peak in $g_{OW-OW}(r)$ increases in magnitude but also shifts to slightly larger distances. This is accompanied by an increase in the magnitude of oscillations at larger distances. The qualitative features of $g_{OW-C}(r)$ do not change with increasing concentration, but the magnitude of the first peak increases dramatically going from 30 to 65 wt %. The correlation between water molecules is more long-ranged than that between water molecules and counterions. We attribute the strong peak in the water−counterion correlation to the correlation between both of these species to the surfactant headgroups in these phases.

The co-ordination number of water molecules, i.e., the number of water molecules near a given water molecule, does not change significantly with concentration. We define the co-ordination number as the number of other water molecules within the first solvation shell, i.e., within a distance corresponding to the first minimum in the radial distribution function. For the different concentrations, the average co-ordination number is 12 (for 0 wt %), 14 (for 30 wt %), 18 (for 65 wt %), and 13 (for 80 wt %). The insensitivity to concentration is surprising given the changes in the radial distribution function. We speculate that this is because the

dx.doi.org/10.1021/jp304933k | J. Phys. Chem. B XXXX, XXX, XXX−XXX

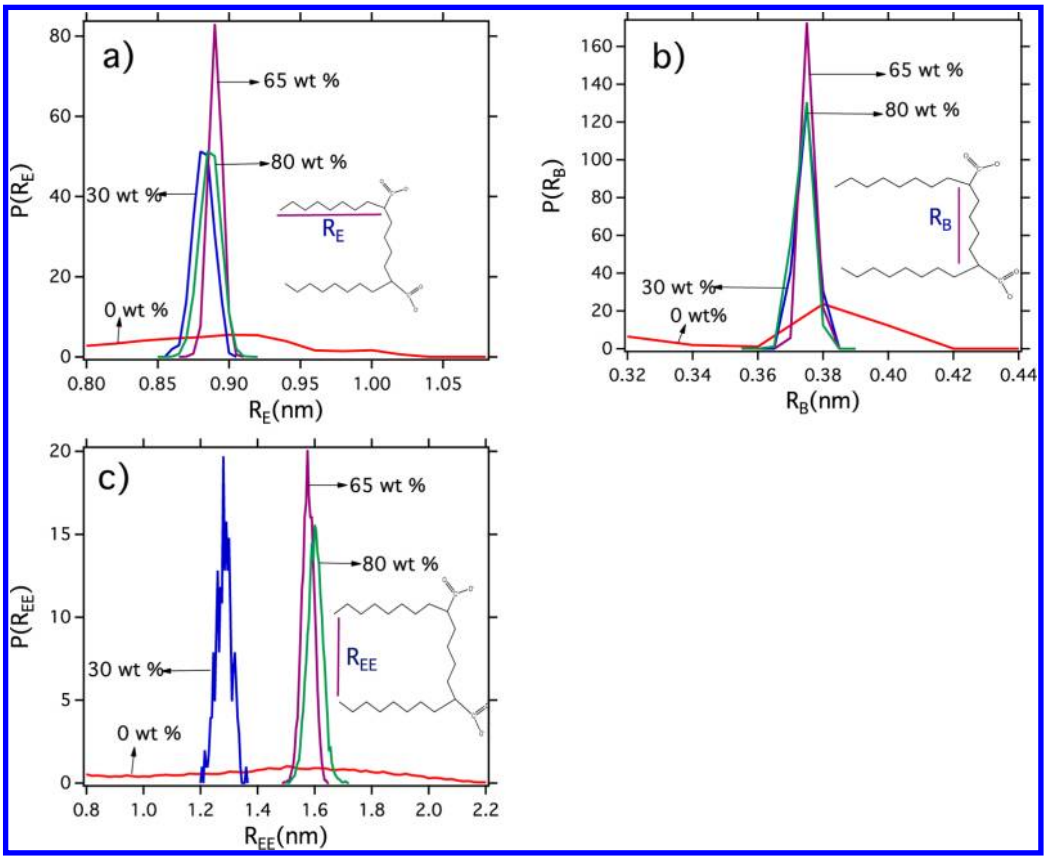

Figure 4. Probability distribution functions of the (a) end-to-end distance of the tails, (b) end-to-end distance of the bridge, and (c) distance between the last site on each tail.

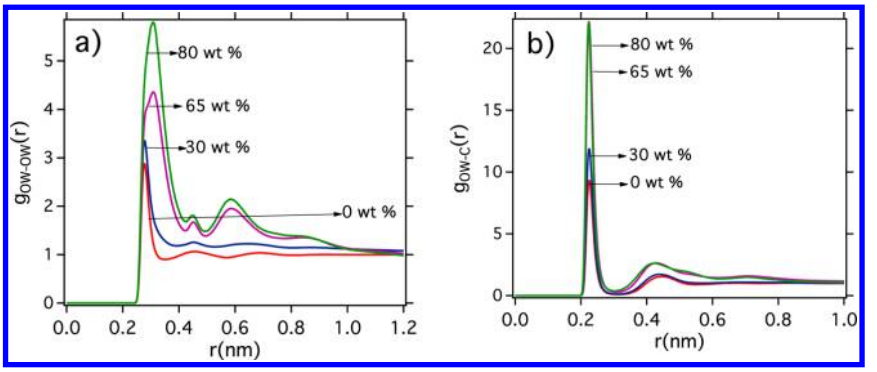

Figure 5. Radial distribution function between the oxygen atom on water molecules and (a) the oxygen atom on other water molecules and (b) counterions.

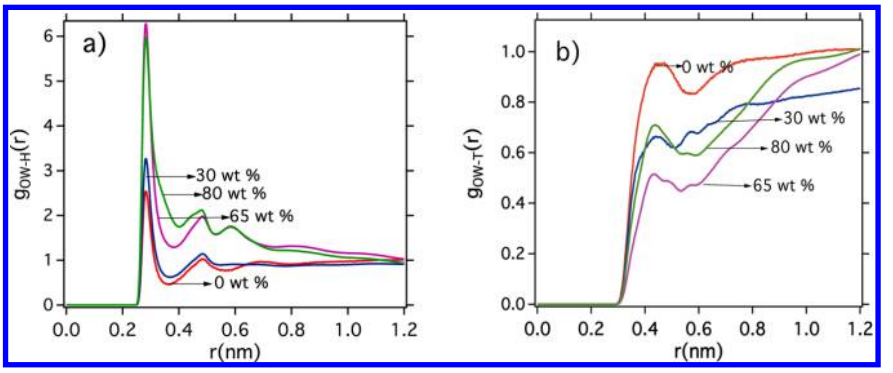

Figure 6. Headgroup−water oxygen and tailgroup−water oxygen radial distribution functions at different concentrations.

dx.doi.org/10.1021/jp304933k | J. Phys. Chem. B XXXX, XXX, XXX−XXX

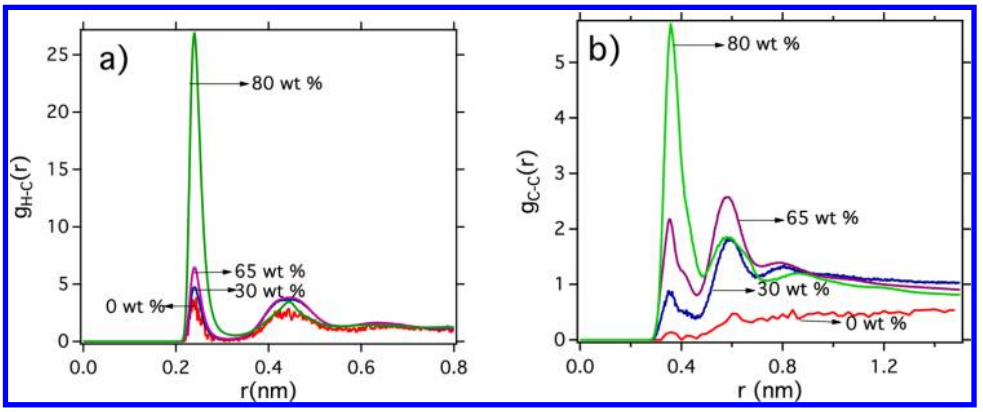

Figure 7. Headgroup−counterion and counterion−counterion radial distribution functions at different concentrations.

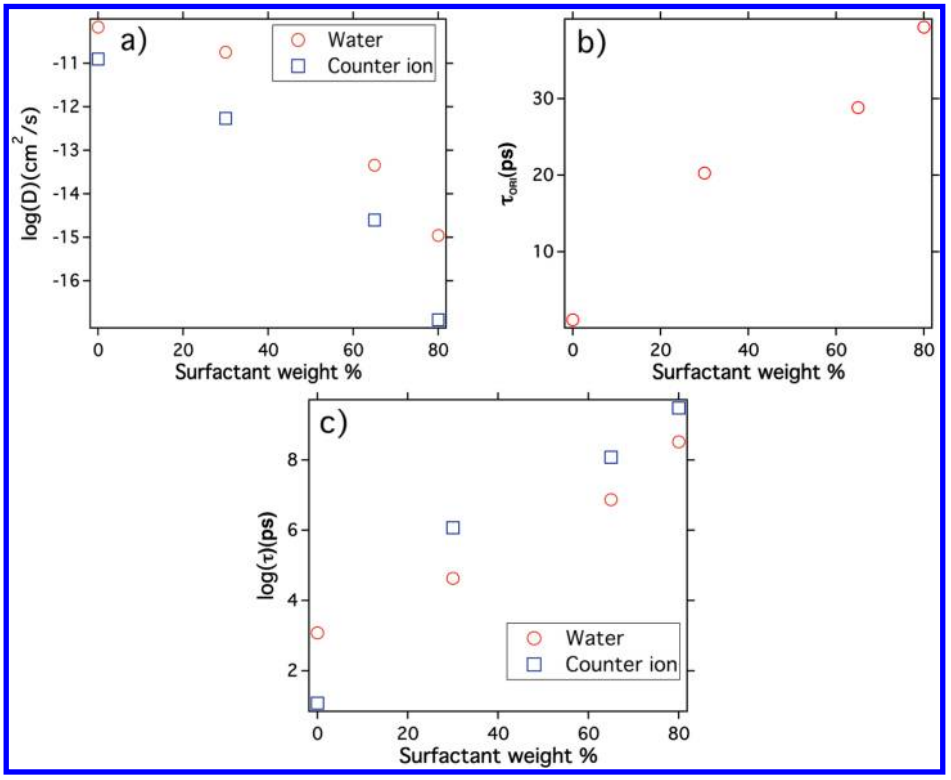

Figure 8. Dynamics of water and counterions: (a) self-diffusion coefficient, (b) orientational relaxation time of water molecules, and (c) residence time of water-oxygen and counterions near the headgroups. Note that the ordinate in parts a and c is on a logarithmic scale.

increase in the value of the radial distribution function is compensated by a decrease in the density of water.

The water molecules are correlated with the headgroups of the surfactants while being excluded from the tail groups. Figure 6 shows the pair correlation function between water and the tail and headgroups of the surfactant. The correlation between headgroups and water increases in lamellar and gyroid phase compared to hexagonal phase and at infinite dilution. This is to be expected because the curvature of the phases becomes less convex. On the other hand, the depletion of water from the region of the tail groups is more significant in the hexagonal phase than in the gyroid and lamellar phases.

The correlation between the counterions and the headgroups (and other counterions) is markedly different in the lamellar phase when compared to the other phases and infinite dilution. This is an important aspect that we think plays an important role in the stability of the lamellar phase. Parts a and b of Figure 7 depict the pair correlation function between the headgroup and the Na^+ counterion and that between counterions, respectively. In all cases, $g_{H-C}(r)$ has two peaks corresponding to a contact ion pair and a solvent separated ion pair. The difference lies in the value of $g_{H-C}(r)$ at the distance corresponding to the contact pair, denoted $g_{contact}$, which increases with increasing surfactant concentration. For infinite dilution, the hexagonal phase, and the gyroid phase, $g_{contact} \approx 2$, 4, and 5, respectively. For the lamellar phase, however, there is a much stronger correlation between the headgroup and the counterion, with $g_{contact} \approx 25$! This dramatic increase cannot be attributed merely to the increase in surfactant concentration but is due to the formation of a curvature free morphology, i.e., lamellar phase.

The build-up of counterions near the headgroups in the lyotropic phases is also reflected in the counterion−counterion pair correlation functions. In the lyotropic phases, there are two

dx.doi.org/10.1021/jp304933k | J. Phys. Chem. B XXXX, XXX, XXX−XXX

peaks in $g_{C-C}(r)$ corresponding to a contact ion pair and a solvent separated ion pair. The magnitude of the peak in the pair correlation function increases with increasing concentration with a dramatic increase going from the gyroid to the lamellar phase. The counterion pair correlation therefore tracks the behavior seen in the counterion−headgroup correlation function. These peaks are, of course, absent at infinite dilution where the counterions repel each other.

The dynamics of counterions and water molecules becomes slower as the concentration is increased. Figure 8 depicts the dynamics of the water molecules and counterions. The self-diffusion coefficient is calculated from the slope of the mean-square displacement, and the orientational relaxation time, τ_{ORI}, is the time integral of the orientational correlation function. As the concentration is increased, the self-diffusion coefficients of the water molecules (D_W) and counterions (D_C) decrease by roughly 2 and 3 orders of magnitude, respectively. The rotational correlation time of the water molecules, however, only increases by a factor of 2. This emphasizes the increasing dynamic heterogeneity in the water dynamics as the concentration is increased and the departure from Stokes−Einstein behavior (where the product $D_W\tau_{ORI}$ is expected to be constant). The greater decrease in D_C (compared to D_W) underscores the impact of the stronger correlations between the headgroups and counterions on the dynamics of the counterions.

The strong correlation between the headgroups and water/counterions is accompanied by a dramatic increase in the residence time of these species near the headgroups. For water, we compute the residence time from the headgroup−solvent/counterion contact autocorrelation function $C_{CH}(t)$ using a protocol previously used by others[37−39] and implemented within the g_hbond tool in Gromacs. A headgroup and solvent molecule or counterions are considered to be in contact if their distance is less than 0.6 nm. The residence time (τ_{SOL}) is the time integral of the autocorrelation function $C_{CH}(t)$.

Figure 8c depicts the residence time of counterions and water molecules in the different phases. The residence time increases by 2−3 orders of magnitude over the range of concentrations studied. For the lamellar phase, the residence time is 5 and 13 ns for water and counterions, respectively, which is astoundingly high. These numbers may be compared to 22 and 3 ps, respectively, at infinite dilution. One can therefore clearly attribute the slower dynamics of these species to the high correlation between the species and the headgroups of the surfactants.

Replacing the Na^+ counterions with TMA^+ counterions results in a transition from a lamellar to a gyroid morphology accompanied by a decrease in the correlation between headgroups and counterions. Starting with the lamellar morphology as an initial configuration, when the Na^+ counterions are changed to TMA^+ counterions, the system spontaneously goes into a gyroid phase over a time scale of 180 ns. Figure 9 depicts the final configuration obtained for the 80 wt % case with TMA^+ counterions, which is clearly a gyroid phase, and looks similar to the morphology in Figure 2b, and very different from the lamellar phase obtained with Na^+ counterions at the same concentration (Figure 2c).

The transition to a gyroid morphology is accompanied by a decrease in the correlation between headgroups and counterion. Figure 10 compares $g_{H-C}(r)$ with Na^+ and TMA^+ counterions. The large size of the TMA^+ counterions causes a first peak at larger distances, and the magnitude of this peak is

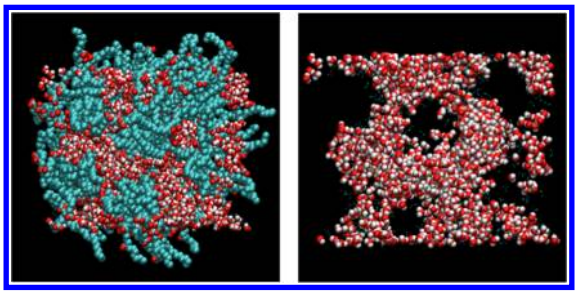

Figure 9. Gyroid phase at 80 wt % of surfactants with TMA^+ counterions.

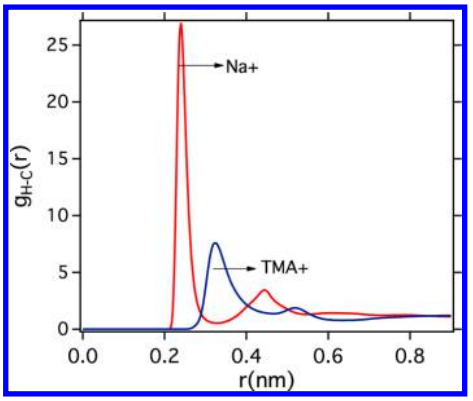

Figure 10. Effect of counterions on headgroup−counterion radial distribution functions at 80 wt % of surfactant concentration.

diminished when compared to the case with Na^+ counterions. The second solvent separated peak is not present with TMA^+ counterions, emphasizing the weaker correlations between TMA^+ counterions and the headgroups. It is possible that the stability of the lamellar phase is due to the strong correlations with the Na^+ counterions. When these electrostatic interactions are weakened (by increasing the size of the counterion), the correlations are diminished and the gyroid phase becomes the stable phase. We therefore speculate that the stability of the gyroid phase is due to electrostatic effects, rather than conformational effects.

The residence time of the TMA^+ counterions near the headgroups is about 8 times smaller than that of the Na^+ counterions, due to the weaker correlations between the TMA^+ and the headgroups.

Considering the strong headgroup−counterion correlations, it is instructive to look at the effect of protonation of the headgroups on the relative stability of the lamellar morphology. Metal carboxylates are basic, and there could be effects of protonation states on the phase stability, as is found experimentally in the micellar limit.[40−42] In all the calculations discussed to this point, all the headgroups are *deprotonated*. In principle, one can include the protonation equilibria using constant pH molecular dynamics, but this is very computationally intensive for the large systems we are interested in. To obtain some insight into the effect of protonation on the phase behavior, we perform simulations with a fraction of headgroups protonated.

To study the effect of protonation on the phase behavior, we use the following protocol. We start with an initial configuration at 80 wt % surfactant with a stable lamellar phase, i.e., similar to the configuration in Figure 2c. We refer to this case as 0% protonation. Initial configurations at other

dx.doi.org/10.1021/jp304933k | J. Phys. Chem. B XXXX, XXX, XXX−XXX

protestation levels are created by choosing the desired number of surfactants randomly and attaching H atoms to both charged oxygen atoms in the carboxylate groups and removing counterions to preserve electroneutrality. Initial configurations are generated in this fashion for 5, 10, and 40% of the surfactants protonated. MD simulations are then run for 300 ns to investigate the stability of the lamellar phase. For 5% protonation, there is little change in the lamellar phase. Figure 11 depicts representative snapshots for 10 and 40% protonation

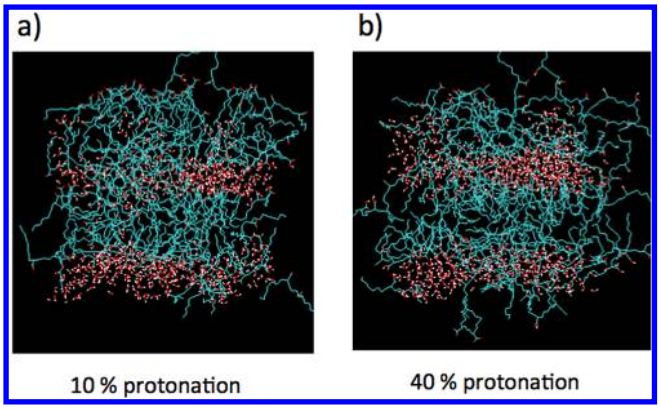

Figure 11. Snapshot of the final configuration (80 wt %) with a degree of protonation of 10 and 40%.

and shows that the lamellar phase possesses less order upon protonation. This emphasizes the importance of electrostatic effects on the stability and degree of order of the lamellar phase.

4. CONCLUSIONS

The self-assembly of a class of gemini surfactants is studied using computer simulations of a united atom model of surfactants and an atomistic model for the water and counterions. As the surfactant concentration is increased, the simulations show a transition from a hexagonal to gyroid to lamellar lyotropic phase, consistent with experiment. The simulations reproduce the experimentally observed morphology at each concentration, suggesting that the force field is reliable.

The conformational properties of the surfactant molecules are relatively insensitive to concentration in the lyotropic phases. This questions the notion that the flexibility of the molecules accommodates the large window of the gyroid phase.

There is, however, a strong correlation between the surfactant headgroups and the counterions and water molecules. The degree of correlation is dramatically higher in the lamellar phase, suggesting that the electrostatic correlations are instrumental in the stability of this phase. In fact, when the Na^+ counterions are replaced with TMA^+ counterions, the lamellar phase is no longer observed (consistent with experiment) because the larger TMA^+ counterions have a weaker electrostatic correlation with the headgroups. The strong static correlation between counterions and surfactant headgroups is accompanied by a dramatic decrease in the self-diffusion of the counterions and water molecules. The rotational relaxation of the water molecules is not significantly changed, however, emphasizing the importance of surfactant−water correlations on the dynamics of the water molecules.

These surfactant systems are an interesting case where the details of chemistry as well as electrostatic interactions affect not only the morphology but also the structural and dynamic properties of the mobile species. They provide the possibility of tuning these features through the chemistry of the molecules. This work shows that computer simulations of these systems are feasible and can be used to predict morphologies and screen for desired properties.

AUTHOR INFORMATION

Corresponding Author

*E-mail: yethiraj@chem.wisc.edu.

Notes

The authors declare no competing financial interest.

ACKNOWLEDGMENTS

This research was supported by the National Science Foundation through the UW-Madison Nanoscale Science and Engineering Center (NSEC) (NSF grant DMR-0832760) and Grant No. CHE-1111835. We thank Greg Sorenson for useful discussions regarding the experiments. This research was supported in part by National Science Foundation Grant CHE-0840494 in the form of generous computing support from UW Madison chemistry department computing cluster. We are grateful for computational support from Abe machine in National Center for Supercomputing Application (NCSA), queen bee machine in LONI supercomputers, and Trestles machine in SDSC supercomputer under grant number TG-CHE090065 and the UW Madison Centre for High Throughput Computing (CHTC) Condor supercomputing facility.

REFERENCES

(1) Fairhurst, C. E.; Fuller, S.; Gray, J.; Holmes, M. C.; Tiddy, G. J. T. In *Handbook of Liquid Crystals*; Demus, D., Goodby, J. W., Gray, G. W., Spiess, H. W., Vill, V., Eds.; Wiley-VCH: Weinheim, Germany, 1998; Vol. 3, pp 341−392.

(2) Kato, T.; Mizoshita, N.; Kishimoto, K. *Angew. Chem., Int. Ed.* **2006**, *45*, 38−68.

(3) Gin, D. L.; Bara, J. E.; Noble, R. D.; Elliott, B. J. *Macromol. Rapid Commun.* **2008**, *29*, 367−389.

(4) Finnefrock, A. C.; Ulrich, R.; Toombes, G. E. S.; Gruner, S. M.; Wiesner, U. *J. Am. Chem. Soc.* **2003**, *125*, 13084−13093.

(5) Shen, S.; Garcia-Bennett, A. E.; Liu, Z.; Lu, Q.; Shi, Y.; Yan, Yu, C.; Liu, W.; Cai, Y.; Terasaki, O.; Zhao, D. *J. Am. Chem. Soc.* **2005**, *127*, 6780−6787.

(6) Rummel, G.; Hardmeyer, A.; Widmer, C.; Chiu, M. L.; Nollert, P.; Locher, K. P.; Pedruzzi, I.; Landau, E. M.; Rosenbusch, J. P. *J. Struct. Biol.* **1998**, *121*, 82−91.

(7) Zhou, M.; Nemade, P. R.; Lu, X.; Zeng, X.; Hatakeyama, E. S.; Noble, R. D.; Gin, D. L. *J. Am. Chem. Soc.* **2007**, *129*, 9574−9575.

(8) Kerr, R. L.; Miller, S. A.; Shoemaker, R. K.; Elliott, B. J.; Gin, D. L. *J. Am. Chem. Soc.* **2009**, *131*, 15972−15973.

(9) Menger, F. M.; Keiper, J. S. *Angew. Chem., Int. Ed.* **2000**, *39*, 1906−1920.

(10) Lynch, M. L.; Spicer, E.; Patrick, T. *Surfactant Sci. Ser.* **2005**, *127*, 1−512.

(11) Sorenson, G. P.; Coppage, K. L.; Mahanthappa, M. K. *J. Am. Chem. Soc.* **2011**, *133*, 14298−14931.

(12) Pindzola, B. A.; Jin, J.; Gin, D. L. *J. Am. Chem. Soc.* **2003**, *125*, 2940−2949.

(13) Czeslik, C.; Winter, R. *J. Mol. Liq.* **2002**, *98*−*99*, 285−293.

(14) Kulkarni, C. V.; Tang, T.-Y.; Seddon, A. M.; Seddon, J. M.; Ces, O.; Templer, R. H. *Soft Matter* **2010**, *6*, 3191−3194.

(15) Matsen, M. W.; Bates, F. S. *Macromolecules* **1996**, *29*, 7641−7644.

(16) Israelachvili, J. N. *Intermolecular and Surface Forces*, 2nd ed.; Academic Press: London, 1991.

(17) Gin, D. L.; Gu, W.; Pindzola, B. A.; Zhou, W.-J. *Acc. Chem. Res.* **2001**, *34*, 973−980.

(18) Karaborni, S.; Esselink, K.; Hilbers, P.; Smit, B.; Karthauser, J.; van, OS, N.; Zana, R. *Science* **1994**, *266*, 254.
(19) Khurana, E.; Nielsen, S.; Klein, M. *J. Phys. Chem. B* **2006**, *110*, 22136.
(20) Almeida, A.; Marques, E.; Jurado, A.; Pais, A. *Phys. Chem. Chem. Phys.* **2010**, *12*, 14462.
(21) Zhao, T.; Xu, G.; Yuan, S.; Chen, Y.; Yan, H. *J. Phys. Chem. B* **2010**, *114*, 5025.
(22) Yi, X.; Jian, F.; Yazhuo, S.; Honglai, L. *Chin. J. Chem. Eng.* **2007**, *15*, 560.
(23) Zhu, S.; Liu, L.; Cheng, F. *Chalcogenide Lett.* **2011**, *8*, 391.
(24) Shinoda, W.; DeVane, R.; Klein, M. *Soft Matter* **2008**, *4*, 2454.
(25) Schuler, L.; Daura, X.; Van Gunsteren, W. *J. Comput. Chem.* **2001**, *22*, 1205.
(26) Berendsen, H. J. C.; Postma, J. P. M.; van Gunsteren, W. F.; Hermans, J. In *Intermolecular Forces*; Pullman, B., Ed.; D. Reidel Publishing Company: Dordrecht, The Netherlands, 1981; pp 331−342.
(27) Krienke, H.; Opalka, D. *J. Phys. Chem. C* **2007**, *111*, 15935.
(28) Hess, B.; Kutzner, C.; Van der Spoel, D.; Lindahl, E. *J. Chem. Theory Comput.* **2008**, *4*, 435.
(29) Miyamoto, S.; Kollman, P. *J. Comput. Chem.* **1992**, *13*, 952.
(30) Darden, T.; York, D.; Pederson, L. G. *J. Chem. Phys.* **1993**, *98*, 952.
(31) Essman, U.; Perera, L.; Berkowitz, M. L.; Darden, T.; Lee, H.; Pederson, L. G. *J. Chem. Phys.* **1995**, *103*, 8577.
(32) Berendsen, H. J. C.; Postma, J. P. M.; DiNola, A.; Haak, J. R. *J. Chem. Phys.* **1984**, *81*, 3684.
(33) Marrink, S.-J.; Mark, A. *Biophys. J.* **2004**, *87*, 3894.
(34) Martínez-Veracoechea, F.; Escobedo, F. *J. Chem. Phys.* **2006**, *125*, 104907.
(35) Cromer, D. T.; Mann, J. *Acta. Crystallogr., Sect. A* **1968**, *24*, 321.
(36) de Vries, A.; Mark, A.; Marrink, S.-J. *J. Am. Chem. Soc.* **2004**, *126*, 4448.
(37) Kim, J.; Yethiraj, A. *J. Phys. Chem. B* **2008**, *112*, 1729.
(38) Makarov, V. A.; Andrews, B. K.; Smith, P.; Pettitt, B. *Biophys. J.* **2000**, *79*, 2966.
(39) Van der Spoel, D.; Van Maaren, P. J.; Larsson, P.; Timneanu, N. *J. Phys. Chem. B* **2006**, *110*, 4393.
(40) Klijn, J. E.; Stuart, M. C. A.; Scarzello, M.; Wagenaar, A.; Engberts, J. B. F. N. *J. Phys. Chem. B* **2006**, *110*, 21694−21700.
(41) Scarzello, M.; Klijn, J. E.; Wagenaar, A.; Stuart, M. C. A.; Hulst, R.; Engberts, J. B. F. N. *Langmuir* **2006**, *22*, 2558−2568.
(42) Klijn, J. E.; Stuart; Scarzello, M.; Wagenaar, A.; Engberts, J. B. F. N. *J. Phys. Chem. B* **2007**, *111*, 5204−5211.